Vibronically Resolved Electronic Circular Dichroism Spectra of (*R*)-(+)-3-Methylcyclopentanone: A Theoretical Study

Na Lin,[†,‡] Fabrizio Santoro,*[,§] Xian Zhao,[‡] Antonio Rizzo,*[,§] and Vincenzo Barone[§]

Department of Theoretical Chemistry, School of Biotechnology, Royal Institute of Technology, SE-10691 Stockholm, Sweden, Institute of Crystal Materials, Shandong University, 250100 Jinan, Shandong, People's Republic of China, and Area della Ricerca, Istituto per i Processi Chimico-Fisici del Consiglio Nazionale delle Ricerche (IPCF-CNR), Via G. Moruzzi 1, I-56124 Pisa, Italy

Received: July 22, 2008; Revised Manuscript Received: September 12, 2008

The vibrationally resolved electronic circular dichroism (ECD) spectra of the two dominant conformers of (*R*)-(+)-3-methylcyclopentanone in gas phase are computed by density functional response theory, with a full account of Franck−Condon and Herzberg−Teller vibrational contributions at the harmonic level. Proper inclusion of the latter contributions was made possible by the recent implementation of effective-scaling computations of vibrational overlaps and of analytical gradients of time dependent DFT. The Coulomb-attenuated Becke three parameters Lee−Yang−Parr (CAM-B3LYP) functional reproduces both the position and the intensity of the experimental peaks, providing a remarkable improvement over the spectra obtained with the popular hybrid B3LYP functional, and allowing a confident assignment of the CD fine vibrational structure. Franck−Condon and Herzberg−Teller contributions are discussed in detail. The computed decrease of the CD intensity in the gas phase upon increase of the temperature of the sample follows the trend observed experimentally in different solvents.

1. Introduction

Circular dichroism (CD) spectroscopy is based on the phenomenon of different absorption of left and right circularly polarized light by a chiral sample. As one of the oldest tools for structural investigation,[1−3] its application to conformational studies relies on correlations between the main CD parameter, the rotatory strength, and molecular structure. Recent advances made on the calculation of CD have greatly enhanced its value for determining absolute configuration of chiral molecules.

Chiral substituted cyclopentanones have attracted much attention due to the interesting conformation of the cyclopentanone ring. In particular, (*R*)-(+)-3-methylcyclopentanone (R3MCP), due to its medicinal potential,[4] has been studied by both experimentalists and theorists.[5−8] Electronic CD (ECD) spectra of R3MCP were recorded and analyzed by Djerassi and co-workers,[9] and later by Richardson[10] and Johnson.[11] Very recently Compton and co-workers made new measurements of the ECD of R3MCP in the vapor[12] and in a long list of solvents.[13] In ref 12 in particular the authors carried out an experimental study of the (2 + 1) resonance enhanced multiphoton ionization CD (REMPICD) of R3MCP. This motivated our ab initio computational study[14] of the one- and two-photon CD spectra of R3MCP, performed within an origin invariant density functional theory (DFT) approximation and accounting for both dominant conformers of the system of interest, the so-called equatorial-methyl (*Eq*) and axial-methyl (*Ax*) structures.[8] The effects of geometry, basis set and choice of functional were carefully analyzed. Nevertheless, all these studies rest on the approximation of vertical excitations, which only give a rough estimate for the band maximum of a transition and cannot deal with experimental spectra showing a pronounced vibrational fine structure. These limitations prompted us to study the vibrationally resolved one-photon ECD for R3MCP in the vapor phase, measured in the experiment[9−12] and not previously discussed.[14] We present, in particular, the application of DFT and its time-dependent extension (TD-DFT) for excited states in combination with an accurate treatment of the vibrational contributions to simulate the vibronic profiles of one-photon ECD of R3MCP, accounting for both Franck−Condon (**FC**) and Herzberg−Teller (**HT**) contributions. Related studies have been performed recently for the ECD spectrum of dimethyloxirane, by Neugebauer and co-workers[15] within the **FC** approximation, and more recently by Nooijen,[16] taking also into account **HT** contributions. Dierksen and Grimme also investigated the role of vibronic **HT** effects in the ECD response of ketones and diketones with an isotopically engendered chirality.[17] All these studies indicated the importance of vibronic coupling effect for CD properties.

The present paper is organized as follows. In section 2 the theoretical methods will be briefly sketched. Computational details follow in section 3. The results of our study are presented and discussed in section 4, whereas section 5 collects our main conclusions.

2. Theory

2.1. General Formalism for ECD Vibrationally Resolved Spectra. The ECD rotatory strength,[18,19] ${}^{g\nu_g f\nu_f}R$, entering the expression of the linear circular dichroism, can be obtained from the imaginary part of the scalar product of the electric dipole and magnetic dipole transition moments,

$$ {}^{g\nu_g f\nu_f}R = \frac{3}{4}\mathrm{Im}[\langle g\nu_g|\hat{u}|f\nu_f\rangle \cdot \langle f\nu_f|\hat{m}|g\nu_g\rangle] \qquad (1) $$

corresponding to a transition between the initial state $|g\nu_g\rangle$ and a final state $|f\nu_f\rangle$. Here ν_g and ν_f label the vibrational states of

* Corresponding authors. E-mail: F.S., f.santoro@ipcf.cnr.it; A.R., rizzo@ipcf.cnr.it.
† Royal Institute of Technology.
‡ Shandong University.
§ Istituto per i Processi Chimico-Fisici del Consiglio Nazionale delle Ricerche.

10.1021/jp8064695 CCC: $40.75
Published on Web 11/11/2008

the electronic states g and f, respectively. Because we work in the frame of harmonic approximation, the vibrational states are direct products of 1D states $|v_{a,n}\rangle$ for each mode a, $|\boldsymbol{v}_n\rangle = |v_{1,n}\rangle \otimes |v_{2,n}\rangle ... \otimes |v_{N,n}\rangle$, where $v_{a,n}$ is the quantum number of $|v_{a,n}\rangle$ and the vector $\boldsymbol{v}_n$ is written as $\boldsymbol{v}_n = (v_{1,n}, v_{2,n}, ..., v_{N,n})$. The α ($\alpha = x, y, z$) Cartesian component of the transition electric dipole moment is evaluated explicitly as

$$\mu^{\alpha}_{gv_g fv_f} = \langle gv_g|\mu_\alpha|fv_f\rangle \tag{2}$$

Integrating eq 2 on the electronic coordinates one obtains

$$\mu^{\alpha}_{gv_g fv_f} = \langle v_g|\mu^{\alpha,e}_{gf}(\mathbf{Q})|v_f\rangle \tag{3}$$

where $\mathbf{Q}$ is the set of normal coordinates and $\mu^{\alpha,e}_{gf}(\mathbf{Q})$ is the so-called electronic transition dipole moment. The latter can be expanded in a Taylor series with respect to the normal coordinates of the ground electronic state ${}^gQ_a$ around the equilibrium geometry ${}^g\mathbf{Q}_0$:

$$\mu^{\alpha,e}_{gf}({}^g\mathbf{Q}) = \mu^{\alpha,e}_{gf}({}^g\mathbf{Q}_0) + \sum_a \frac{\partial \mu^{\alpha,e}_{gf}}{\partial {}^gQ_a} {}^gQ_a + \cdots \tag{4}$$

Inserting this expansion, limited to the first two terms, into eq 3 yields

$$\mu^{\alpha}_{gv_g fv_f} = \mu^{\alpha,e}_{gf}({}^g\mathbf{Q}_0)\langle v_g|v_f\rangle + \sum_a \frac{\partial \mu^{\alpha,e}_{gf}}{\partial {}^gQ_a}\langle v_g|{}^gQ_a|v_f\rangle \tag{5}$$

The first quantity on the right-hand side is the electronic transition moment of the initial state at the equilibrium position of the ground electronic state, multiplied by the **FC** overlap. The second term arises from the vibronic coupling between different electronic states and it yields the so-called **HT** contribution. Notice that the $\langle v_g|{}^gQ_a|v_f\rangle$ matrix elements are easily traced back to combinations of overlaps between vibrational states.[20] Similarly, we can also obtain an expression for the magnetic dipole operator

$$m^{\alpha}_{gv_g fv_f} = m^{\alpha,e}_{gf}({}^g\mathbf{Q}_0)\langle v_g|v_f\rangle + \sum_a \frac{\partial m^{\alpha,e}_{gf}}{\partial {}^gQ_a}\langle v_g|{}^gQ_a|v_f\rangle \tag{6}$$

In the following we will report results for the anisotropy of the molar absorptivity $\varepsilon(\omega)$, a function of the laser frequency ω, defined as the difference between the absoptivity for left (L) and right (R) circularly polarized light, which can be written as[14]

$$\begin{aligned}\Delta\varepsilon(\omega) &= \varepsilon_L(\omega) - \varepsilon_R(\omega)\\ &= \frac{64\pi^2\omega N_A}{9\times 1000\times \ln(10)\times(4\pi\varepsilon_0)\times\hbar c_0{}^2}\times\\ &\sum_f \sum_{v_g,v_f} p_{v_g} g(\omega, \omega_{gv_g fv_f})\times {}^{gv_g fv_f}R\\ &= \frac{64\pi^2\omega N_A}{9\times 1000\times \ln(10)\times(4\pi\varepsilon_0)\times\hbar c_0{}^2}\times \sum_f {}^{gf}R(\omega)\\ &\approx 2.73719\times 10^{-2}\times\omega\sum_f {}^{gf}R(\omega)\end{aligned} \tag{7}$$

Above $\omega_{gv_g fv_f}$ is the transition energy from $|gv_g\rangle$ to $|fv_f\rangle$, $g(\omega,\omega_{gv_g fv_f})$ is the line shape function, N_A is Avogadro's number, c_0 is the speed of light in vacuo and ε_0 is the vacuum permittivity. p_{v_g} is the Boltzmann population of initial vibrational state $|v_g\rangle$. Our spectra are computed from the vibrational ground state, which is dominant in the Boltzmann distribution. Anisotropies in dm^3 mol^{-1} cm^{-1} are obtained employing the expression in the last line of eq 7 when ω, $\omega_{gv_g fv_f}$ and ${}^{gv_g fv_f}R$ are given in atomic units.

2.2. Analytical Sum Rules for Total Intensity. Consider eq 7 and let us introduce the total rotatory strength of the ECD transition $g \rightarrow f$, ${}^{gf}R = \int {}^{gf}R(\omega)\, d\omega$. In the limit of first-order expansion in eqs 5 and 6, and assuming completeness of the vibrational-state manifold (holding in the exact limit), we can write

$$\begin{aligned}{}^{gf}R &= \frac{3}{4}\sum_{v_g,v_f} p_{v_g}\mathrm{Im}\langle v_g|\mu^e_{gf}({}^g\mathbf{Q})|v_f\rangle\cdot\langle v_f|m^e_{gf}({}^g\mathbf{Q})|v_g\rangle\\ &= \frac{3}{4}\sum_{v_g} p_{v_g}\mathrm{Im}\langle v_g|\mu^e_{gf}({}^g\mathbf{Q})\cdot m^e_{gf}({}^g\mathbf{Q})|v_g\rangle\\ &= \frac{3}{4}\sum_{\alpha=x,y,z}\sum_{v_g} p_{v_g}\mathrm{Im}\langle v_g|[\mu^{\alpha,e}_{gf}({}^g\mathbf{Q})m^{\alpha,e}_{gf}({}^g\mathbf{Q})]|v_g\rangle\\ &= \frac{3}{4}\sum_{\alpha=x,y,z}\sum_{v_g} p_{v_g}\mathrm{Im}\langle v_g|\{[\mu^{\alpha,e}_{gf}({}^g\mathbf{Q}_0) +\\ &\sum_a \frac{\partial \mu^{\alpha,e}_{gf}}{\partial {}^gQ_a}{}^gQ_a]\times[m^{\alpha,e}_{gf}({}^g\mathbf{Q}_0) + \sum_b \frac{\partial m^{\alpha,e}_{gf}}{\partial {}^gQ_b}{}^gQ_b]\}|v_g\rangle\end{aligned} \tag{8}$$

Because expectation values of the linear terms ${}^gQ_a$ or ${}^gQ_b$, as well as those of the nondiagonal bilinear terms ${}^gQ_a{}^gQ_b$ with $a \neq b$, vanish, leaving under our approximation only expectation values of ${}^gQ_a{}^2$, for each final electronic state f we can obtain

$$\begin{aligned}{}^{gf}R &= \frac{3}{4}\sum_{\alpha=x,y,z}\mathrm{Im}\left[\mu^{\alpha,e}_{gf}({}^g\mathbf{Q}_0)m^{\alpha,e}_{gf}({}^g\mathbf{Q}_0) +\right.\\ &\left.\sum_a\sum_{v_g} p_{v_g}\frac{\partial \mu^{\alpha,e}_{gf}}{\partial {}^gQ_a}\frac{\partial m^{\alpha,e}_{gf}}{\partial {}^gQ_a}\frac{\hbar}{2\omega_a}(2v_{a,g}+1)\right]\\ &= {}^{gf}R^{\mathbf{FC}} + {}^{gf}R^{\mathbf{HT}}\end{aligned} \tag{9}$$

where ω_a is the harmonic frequency of mode a. The first term in the square brackets corresponds to the total **FC** intensity, and it is the standard expression for the vertical-transition rotatory strength, whereas the second term correlates with the total **HT** intensity. Equation 9 is therefore a generalization of the standard (**FC**) expression of the rotatory strength to include **HT** effects, and it highlights two interesting features: (i) mixed terms, **FC** in μ (m) and **HT** in m (μ), do not contribute to the total intensity; (ii) though the **FC** contribution of a single conformer to the total intensity does not depend on temperature, the **HT** one in principle does, through the vibrational quanta $v_{a,g}$ and the Boltzmann weights p_{v_g}.

2.3. Vibrational Contributions. As shown in eqs 5−7, and in ref 20 the computation of ECD vibronic intensities can be traced back to overlaps of multidimensional vibrational states. In the present work vibrations are treated in the frame of harmonic approximation. The sets of normal coordinates of the electronic states g and f, represented by the column vectors ${}^g\mathbf{Q}$ and ${}^f\mathbf{Q}$, respectively, are related by the linear transformation

$${}^g\mathbf{Q} = \mathbf{J}{}^f\mathbf{Q} + \mathbf{K} \tag{10}$$

where $\mathbf{J}$ is the so-called Duschinsky matrix and $\mathbf{K}$ is the column vector of the displacements of the equilibrium geometry (from f to g).[21] We obtain $\mathbf{J}$ and $\mathbf{K}$ by locating the equilibrium structures of both states involved in the transition via direct geometry optimization and by performing a harmonic analysis

of both potential energy surfaces (PESs), each around the corresponding equilibrium position. **J** and **K** are then easily obtained as described in refs 22 and 23. In the literature our approach has been sometimes defined by Hazra, Nooijen and co-workers as "harmonic adiabatic **FC** approach" (AFC),[24,25] to be distinguished from a different approach, known as "harmonic vertical hessian **FC** approach" (HFC)[24,25] where the excited PES is characterized by the calculation of the full Hessian at the equilibrium geometry of the ground state (**FC** geometry). In the limit of an exactly harmonic excited PES the two approaches are equivalent, whereas in all the realistic cases where anharmonicities exist they are different. In the latter cases, AFC provides a better description and assignment of high-resolution spectra, especially in their low energy part, whereas HFC is more suited for a proper description of the low-resolution features of the spectra and of the region of the maximum band. The two approaches may yield sensibly different predictions when relevant anharmonicities play a role. Only the reliable treatment of these anharmonicities, which is hardly feasible for sizable molecule, can provide a clear-cut improvement of the spectrum description. In these cases, remaining within the realm of harmonic models, only an ad hoc study on the specific system can tell which between AFC and HFC approaches performs better.

In general the matrix **J** is not diagonal, which means that normal modes are mixed by an optical transition. In principle, this fact severely increases the burden for the computation of $\mu_{gv_gfv_f}$ and $m_{gv_gfv_f}$, because multidimensional overlaps $\langle v_g|v_f\rangle$ cannot be reduced to the product of one-dimensional integrals. Effective recursive formulas to compute these overlaps have been obtained (see, for instance, Kupka et al.[26] and Peluso et al.[22]) on the basis of the seminal papers by Sharp et al.[27] and Doktorov et al.[28] For sizable molecules, an additional difficulty arises, because the number of vibronic transitions to be taken into account is in principle very large, making a brute force computation practically unfeasible. Some of us[23,29] have recently developed an effective method for the computation of **FC** spectra of large molecules, based on a partition of the manifold of the possible vibronic transitions in classes, *Cn*, depending on the number *n* of simultaneously excited modes, and on an effective and automatic method for the selection of the relevant vibronic transitions. This method, implemented in the FORTRAN code **FC***classes*,[30] has been very recently extended to deal with the more general case of linear dependence of the transition dipole moment on the normal coordinates (**HT** effect),[20] showing that selection schemes only tailored to obtain converged **FC** spectra may fail in the case of **HT** spectra.

The computation of AFC harmonic spectra requires therefore the often cumbersome determination of the equilibrium structure and a harmonic analysis of all the excited electronic states spanning the energy window of interest. A noticeable simplification is introduced by expanding the difference between the final and ground-state potentials around the **FC** geometry and by cutting the expansion at the first-order (linear) terms. The underlying model assumes that normal modes and frequencies are the same in the initial and final electronic states of the transition while equilibrium geometries are displaced. In this framework, the displacements can be simply derived from the excited PES gradients (obtainable by numerical derivation) at the **FC** geometry. As a consequence, the model has been sometimes defined as a gradient **FC** (GFC) approach.[16] Macak et al.[31] used for this model the acronym "LCM", standing for linear coupling model, and introduced also **HT** effects through the evaluation of numerical derivatives of the relevant transition properties at the **FC** geometry. LCM neglects the effects of the Duschinsky rotation of the normal coordinates[21] (which corresponds to setting $\mathbf{J} = \mathbf{1}$ in eq 10), as well as those of the possible change of frequencies in the different electronic states, and it has been widely and successfully adopted to account for the effect of molecular vibrations for many systems and several one- and two-photon absorption and photon-emission processes.[32−38]

Although LCM generally provides good low-resolution spectra, it is not fully adequate to simulate and interpret (in terms of assignment of the main vibrational bands) well resolved optical spectra because, in that case, the position of the peaks is dictated by the frequencies of the final electronic state, which are in general different from those of the ground state. In the present work we consider an energy window covering the first six singlet excited states of R3MCP, as obtained in a TDDFT calculation. Experimental ECD data are only available for the two lowest, S1 and S2 states ranging from 185 to 345 nm, and they are nicely resolved.[12] Therefore we compute both harmonic AFC and LCM spectra for the first two excited states, and we resort to the less expensive LCM to describe the ECD response of the S3−S6 excited states.

3. Computational Details

In this paper the vibronically resolved ECD spectra yielded by the first six excited electronic states, S1−S6, of the two lowest lying conformers identified for gaseous R3MCP, the *Eq* and *Ax* forms (see Figure 1 in ref 8 and in ref 14), are computed. Geometry optimization, as well as the calculation of the vibrational normal modes of the electronic ground state, was carried out using GAUSSIAN 03[39] at the DFT level, based on the hybrid Becke three parameters Lee−Yang−Parr (B3LYP) functional.[40−42] The transition dipole moments, their derivatives, and the excited-state energy gradients for LCM were calculated with both the DFT/B3LYP and recent Coulomb-attenuated-B3LYP DFT/CAM-B3LYP[43,44] methods. In our calculation, the standard parametrization ($\alpha = 0.190$, $\beta = 0.460$, $\mu = 0.330$) was used for CAM-B3LYP. The DALTON 2.0 chemistry program[45] was employed. For all these quantum-chemical calculations the triple-ζ augmented correlation consistent aug-cc-pVTZ basis set (552 bf) was used. For the S1 and S2 states a full optimization of the equilibrium geometry was performed together with the calculation of the vibrational normal modes employing the CAM-B3LYP functional and the more affordable aug-cc-pVDZ basis set, using in this case a development version of GAUSSIAN.[46] Excited-state minima energies were then refined at the CAM-B3LYP/aug-cc-pVTZ level.

The Boltzmann averaging was performed using calculated free energy changes ΔG_i^0 (at 298.15 K and 1 atm) and the property $P_i(\omega)$ for the two conformations of the molecule. The Boltzmann averaged spectrum is then calculated from

$$P^{\mathrm{avg}}(\omega) = \sum_{i=eq,ax} P_i(\omega) X_i \tag{11}$$

$$X_i = \frac{\exp \dfrac{-\Delta G_i^0}{kT}}{\sum_{i=eq,ax} \exp \dfrac{-\Delta G_i^0}{kT}} \tag{12}$$

Above, k and T are the Boltzmann constant and the temperature in Kelvin, respectively, and $\Delta G_i^0 = G_i^0 - G_0^0$, with G_0^0 as Gibbs free energy of the lowest lying conformer. Gibbs free energies calculated with B3LYP/aug-cc-pVTZ are −309.889597 au and

TABLE 1: Vertical Excitation Energy E^e_{gf} (eV), One-Photon Wavelength λ^e_{gf} (nm), and Vertical Excitation Circular Dichroism Rotatory Strength ${}^{gf}R^e$ (10^{-3} au) for Each of the Six Lowest Excited States of the Equatorial-Methyl (*Eq*) and Axial-Methyl (*Ax*) Conformers of R3MCP[a]

Eq				*Ax*			
state	E^e_{gf}	λ^e_{gf}	${}^{gf}R^e$	state	E^e_{gf}	λ^e_{gf}	${}^{gf}R^e$
B3LYP/aug-cc-pVTZ							
S1	4.22	294.0	18.8110	S1	4.20	295.3	−15.9867
S2	5.64	219.7	−17.7565	S2	5.59	221.6	1.3668
S3	6.11	202.9	2.1614	S3	6.13	202.2	−1.8390
S4	6.15	201.7	−0.2790	S4	6.22	199.2	2.1257
S5	6.26	198.0	1.2315	S5	6.28	197.4	−8.7536
S6	6.80	182.4	14.7383	S6	6.82	181.8	−4.7890
CAM-B3LYP/aug-cc-pVTZ							
S1	4.30	288.5	14.5345	S1	4.28	289.5	−13.1151
S2	6.33	195.7	−14.7405	S2	6.32	196.1	−1.0470
S3	6.86	180.8	0.9563	S3	6.89	180.0	−4.5549
S4	7.03	176.4	0.3550	S4	7.06	175.7	−0.8800
S5	7.06	175.7	4.8909	S5	7.08	175.0	−2.3387
S6	7.61	162.9	14.8717	S6	7.63	162.5	−4.2682

[a] Both B3LYP/aug-cc-pVTZ and CAM-B3LYP/aug-cc-pVTZ results are presented.

−309.887534 au for the gas phase *Eq* and *Ax* conformers, respectively. The Boltzmann percentages of the two conformers in the gas phase computed in this way are therefore 89.9% and 10.1%, for the equatorial and axial forms, respectively, as also found out by the authors of ref 8.

All the ECD spectra reported in this work were computed with a modified version of the code **FC***classes*,[30] specifically tailored to obtain fully converged ECD spectra. For spectra involving the S3−S6 states, **FC***classes* was further modified to provide LCM spectra; therefore also the **FC** integrals needed for LCM spectra are computed from recurrence formulas derived for the full-harmonic case.[23,29] The convergence of the calculation was carefully checked both considering the spectral profiles and the convergence of the sum of the state-to-state rotatory strengths in eq 1 to the analytical sum of eq 9.

4. Results and Discussion

4.1. LCM Analysis. ***4.1.1. Performance of the Functionals: B3LYP vs CAM-B3LYP.*** A detailed comparison between the "vertical-transition" results, i.e. transitions between the electronic states without taking the vibrational states into account (the symbols for the corresponding quantities are labeled by a superscript *e*), obtained with the B3LYP and CAM-B3LYP functionals was already made in a previous work by some of us.[14] Here we just summarize the most important conclusions.

Calculated vertical excitation energy E^e_{gf}, one-photon wavelength λ^e_{gf}, and circular dichroism rotatory strength ${}^{gf}R^e$ (${}^{gf}R^e \equiv {}^{gf}R^{FC}$) for each of the six lowest excited states of the *Eq* and *Ax* conformers of R3MCP are presented in Table 1; see also ref 14. Both B3LYP/aug-cc-pVTZ and CAM-B3LYP/aug-cc-pVTZ results are given. All calculations are performed on the B3LYP/aug-cc-pVTZ optimized geometries of the ground electronic state. Note that the very small differences with respect to the data included in Table 4, p 164312 of ref 14 result from the fact that in this work the structures were reoptimized, instead of being taken from the Supporting Information coming with ref 8 (as done in ref 14).[47]

The data in Table 1 show that different choices of functionals affect remarkably both the position and intensity of the ECD rotatory strength. Excitation energies are consistently larger for

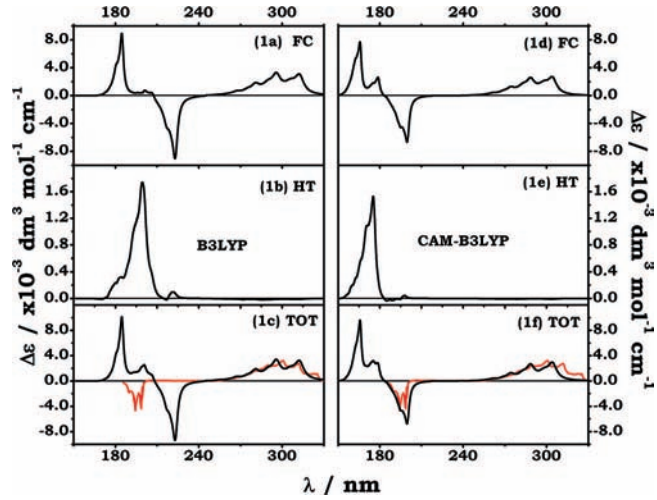

Figure 1. Vibronically resolved Boltzmann averaged (T = 298.15 K, P = 1 atm) circular dichroism spectra of vapor phase R3MCP, calculated within the linear coupling model (LCM). Both B3LYP/aug-cc-pVTZ (panels a−c) and CAM-B3LYP/aug-cc-pVTZ (panels d−f) results, on the basis of B3LYP/aug-cc-pVTZ optimized geometries and summing over the first six excited states of the two major gas phase conformers (equatorial-methyl and axial-methyl), are reported. Franck−Condon (**FC**) and Herzberg−Teller (**HT**) contributions, as well as the total (**TOT** = **FC** + **HT**) spectra are shown with lifetime broadening of 0.05 eV. The red line corresponds to the experimental spectrum; see refs 12 and 13.

both conformers with CAM-B3LYP, by about 0.08 eV for the first excited state, usually identified as an $n \rightarrow \pi^*$ transition. The other five states placed in the wavelength range between 220 and 180 nm by B3LYP, are shifted to the 200−160 nm region by CAM-B3LYP. This is the area where the lowest lying members of the $n \rightarrow s$, $n \rightarrow p$, and $n \rightarrow d$ Rydberg series in both *Eq* and *Ax* conformers lie.[48] In this region the CAM-B3LYP functional yields a far better agreement than B3LYP with the experimental peak positions, whereas B3LYP instead appears to be consistently off the region of the Rydberg series by approximately 20 nm. The rotatory strength ${}^{gf}R^e$ also feels the effect of different functionals, as it is clearly seen from Table 1, and in some cases a change of sign when switching between the two functionals is observed.

Skomorowski and co-workers[49] have already pointed out that the CAM-B3LYP functional improves considerably on B3LYP, yielding results usually obtainable with more sophisticated ab initio approaches as coupled cluster singles and doubles (CCSD) or extended active space multiconfigurational self-consistent field, in studies of ECD spectra of some disulphide chromophores. Similar evidence was given by our previous work on R3MCP.[14] The importance of the choice of parametrization of the CAM-B3LYP functional for the calculation of linear and nonlinear rotatory strengths has been discussed.[50,51] It was found that most of these parametrizations yield results not only better than B3LYP but also better than those obtained with the standard CAM-B3LYP selection. Note, however, that, as pointed out in ref 14, R3MCP involves more Rydberg-like states than those of the systems investigated in ref 51 and the conclusions of Shcherbin and Ruud in ref 51 cannot be therefore easily extended to the present case.

In Figure 1 we report the LCM vibronically resolved Boltzmann averaged (T = 298.15 K, P = 1 atm) circular dichroism spectra of vapor phase R3MCP, calculated both with B3LYP/aug-cc-pVTZ (panels a−c) and CAM-B3LYP/aug-cc-pVTZ (panels d−f) with B3LYP/aug-cc-pVTZ optimized geometries, in a region of wavelengths encompassing the

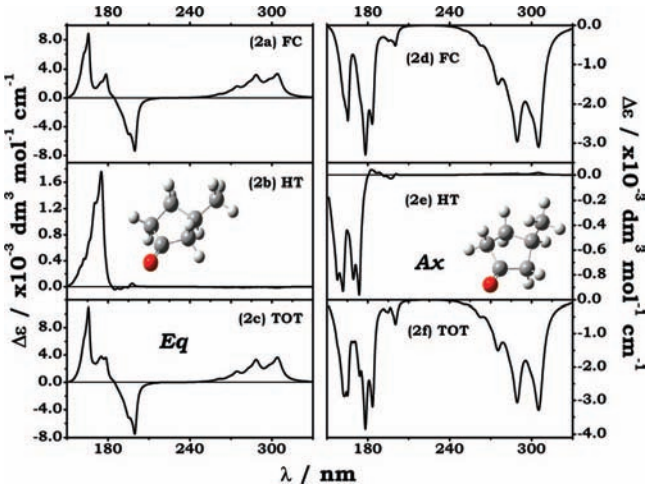

Figure 2. Vibronically resolved circular dichroism spectra of the equatorial-methyl (*Eq*, panels a−c) and axial-methyl (*Ax*, panels d−f) conformers of R3MCP. The linear coupling vibronic model (LCM) was employed. CAM-B3LYP/aug-cc-pVTZ property calculations carried out on B3LYP/aug-cc-pVTZ optimized geometries, summing over the first six excited electronic states. Franck−Condon (**FC**) and Herzberg−Teller (**HT**) contributions, together with the total (**TOT** = **FC** + **HT**) spectra are shown with lifetime broadening of 0.05 eV.

response of the first six excited electronic states. **FC**, **HT** as well as total (**TOT** = **FC** + **HT**) spectra are shown. An "experimentally reasonable" broadening lifetime of 0.05 eV was adopted. The red line corresponds to the experimental spectrum, see ref 12.

The vibronically resolved spectra show pronounced fine structures around each vertical electronic excitation, in particular for the lowest-lying transition S1. As far as integrated intensities (the numerical integration of the spectrum over the whole explored energy range) are concerned, the *Eq*:*Ax* ratio is approximately 2:1.1. By also taking into account the 9:1 ratio coming from the Boltzmann distribution, it is apparent that the *Eq* conformer largely dominates the CD spectra. The main difference between the spectra obtained with B3LYP and CAM-B3LYP is the energy shift of the S2−S6 region; see what we have discussed above for the "vertical-transition" CD. Apparently, cf. bottom panels, the CAM-B3LYP result shows better agreement both for the experimental peaks position and for the intensities. Comparing the **FC** spectra, panels a and d in Figure 1, weaker intensities are obtained with CAM-B3LYP with respect to B3LYP for the first two excited states, whereas a larger intensity is observed for S5. In the S1 region, the long vibrational progression mainly comes from **FC**, with rather negligible **HT** contributions. S4 is responsible for the largest peak in the **HT** spectra for both functionals. The **HT** effect becomes even larger than the **FC** part, resulting in a shoulder in the total spectra.

4.1.2. Eq vs Ax and FC vs HT. In the following sections we focus our attention on the CAM-B3LYP results, which were shown to be in better agreement with the experiment. In Figure 2 we report the CAM-B3LYP/aug-cc-pVTZ vibronic resolved profiles for the CD spectra of the *Eq* (panels a−c) and *Ax* (panels d−f) conformers of R3MCP, obtained within the LCM vibronic model. The calculated **FC** and **HT** contributions, as well as the total spectra combining the two effects (**TOT**), are shown in the energy region of the first six excited states. As above, a broadening lifetime of 0.05 eV is adopted.

In the S1 region, panel c vs f, *Eq* shows a large positive ECD signal with a long vibrational progression, whereas the *Ax* conformer gives a negative, relatively less intense band in the same area. S2 yields a negative band in the *Eq* conformer, whose absolute intensity is comparable with that seen for S1, and a much less intense negative band for the *Ax* conformation. The S3−S6 states are very close in energy, and together they give rise to a positive signal in *Eq* and a negative one for *Ax*. In total, the *Ax* conformer shows weaker ECD intensities compared with *Eq*.

TABLE 2: Total Franck−Condon ($^{gf}R^{FC}$) and Herzberg−Teller ($^{gf}R^{HT}$) Intensities (Unit: 10^{-3} au) for the First Six Excited States of Both Equatorial-Methyl (*Eq*) and Axial-Methyl (*Ax*) Conformers of R3MCP, Evaluated Using Eq 9 with a CAM-B3LYP/aug-cc-pVTZ Approach[a]

	Eq				*Ax*			
state	$^{gf}R^{FC}$	conv	$^{gf}R^{HT}$	conv	$^{gf}R^{FC}$	conv	$^{gf}R^{HT}$	conv
S1	14.5345	100	−0.0729	99.9	−13.1151	100	0.0712	99.9
S2	−14.7405	100	−0.0310	99.7	−1.0470	100	0.0066	98.9
S3	0.9563	100	−0.1316	98.2	−4.5549	99.9	0.2621	99.0
S4	0.3550	100	3.7523	99.9	−0.8800	100	−1.3883	99.9
S5	4.8909	100	0.1454	100	−2.3387	100	−0.8939	99.6
S6	14.8717	100	0.6371	99.6	−4.2682	100	−2.0481	99.4

[a] The convergence (%) of the calculation is also reported; see text.

For both conformers, the **FC** contribution dominates. The **HT** contribution is essentially imperceptible in the range of wavelengths where state S1 absorbs. Differently from **FC**, the essence of the **HT** contribution lies in the well-known "borrowing-mechanism", where intensity is borrowed from other states close-by in energy.[52−54] We have shown elsewhere[32] that the necessary precondition for a strong **HT** contribution in the absorption spectra of a given excited state is the presence of other states close in energy and exhibiting a large intensity. For weak transitions, the **HT** contribution can be as strong, and even larger than the **FC** term. Due to the geometry dependence of the transition moments entering eqs 5 and 6, it may happen that vibrational transitions which are forbidden through a direct electronic transition mechanism, gain intensity due to the mixing of electronic diabatic states. Moreover, in ECD spectra involving delicate cancelations of positive and negative contributions the **HT** term behaves in a far more complex way than for the corresponding absorption spectra. In R3MCP, S1 lies far away from the other five states, with a separation of ≈93 nm (CAM-B3LYP, reducing to ≈74 nm with B3LYP) from its closest neighbor S2. Because large energy separations hamper the coupling between the states, the intensity S1 can borrow from others is very limited, and as a result its **HT** contribution is essentially vanishing. The other five states are all rather close in energy. This results in strong couplings between them, which, together with the mechanism of cancelations of positive and negative intensities, make the analysis of the **HT** effect for each of these five excited states quite complex.

An easy way to compare directly **FC** and **HT** is through the total intensities, which can be discussed for a given transition on the basis of the analytical sums introduced in eqs 8 and 9. Note, however, that total **HT** intensity may in principle have both positive and negative contributions, and therefore the actual relevance of the **HT** effect for the spectrum profile may be ill-estimated by an analysis of $^{gf}R^{HT}$ only. The calculated total **FC** and **HT** intensities obtained by using eq 9 with the CAM-B3LYP/aug-cc-pVTZ approach for both the *Eq* and *Ax* conformers are given in Table 2. The convergence of the spectra calculations for each final state *f* is also reported, as the ratio between the sum of the intensities of the state-to-state rotatory strength $^{g\nu_g f\nu_f}R$ explicitly considered in the computation of the

TABLE 3: Frequency ω_a, Potential Displacement d_a, Energy Shift ΔE, and Franck−Condon Factors of the Most Important Vibrational Modes for the CD Spectra of the Equatorial-Methyl Conformer of R3MCP, Calculated with CAM-B3LYP/aug-cc-pVTZ Approach[a]

	mode	ω_a (cm^{-1})	d_a (au)	ΔE (cm^{-1})	$\|\langle 0\|0\rangle\|^2$	$\|\langle 0\|1\rangle\|^2$	$\|\langle 0\|2\rangle\|^2$		mode	ω_a (cm^{-1})	d_a (au)	ΔE (cm^{-1})	$\|\langle 0\|0\rangle\|^2$	$\|\langle 0\|1\rangle\|^2$	$\|\langle 0\|2\rangle\|^2$
S1	8	538	−9	−52	0.91	0.09	0.00	**S2**	8	538	−12	−99	0.83	0.15	0.01
	9	585	−8	−49	0.92	0.08	0.00		10	725	8	−82	0.89	0.10	0.01
	10	725	−12	−169	0.79	0.18	0.02		22	1222	−4	−43	0.97	0.03	0.00
	13	890	5	−38	0.96	0.04	0.00		23	1254	−4	−56	0.96	0.04	0.00
	15	951	2	−11	0.99	0.01	0.00		24	1269	4	−52	0.96	0.04	0.00
	16	996	−3	−19	0.98	0.02	0.00		25	1304	6	−126	0.91	0.09	0.00
	19	1145	2	−14	0.99	0.01	0.00		26	1320	4	−55	0.96	0.04	0.00
	35	1806	13	−1317	0.48	0.35	0.13		35	1806	−5	−197	0.90	0.10	0.01
S5	8	538	−9	−52	0.91	0.09	0.00	**S6**	5	409	−10	−37	0.91	0.08	0.00
	10	725	6	−50	0.93	0.06	0.00		8	538	−7	−35	0.94	0.06	0.00
	19	1145	4	−58	0.95	0.05	0.00		10	725	11	−145	0.82	0.16	0.02
	22	1222	−4	−52	0.96	0.04	0.00		23	1254	−4	−47	0.96	0.04	0.00
	23	1254	−4	−47	0.96	0.04	0.00		25	1304	5	−91	0.93	0.07	0.00
	24	1269	3	−44	0.97	0.03	0.00		26	1320	4	−55	0.96	0.04	0.00
	25	1304	5	−91	0.93	0.07	0.00		27	1347	−3	−35	0.97	0.03	0.00
	35	1806	−5	−175	0.91	0.09	0.00		35	1806	−5	−197	0.90	0.10	0.01

[a] Only the S1, S2, S5 and S6 states are analyzed, because the intensity for states S3 and S4 is essentially vanishing.

spectrum (taking into account only either the **FC** or the **HT** contribution) and the total analytical intensities ${}^{gf}R^{\mathbf{FC}}$ and ${}^{gf}R^{\mathbf{HT}}$, respectively; see eq 9. Very satisfactory levels of convergence are obtained for both **FC** and **HT**. Convergence is excellent also for **TOT**, to a level always intermediate between those of the **FC** and **HT** terms (and closer to that of the **FC** one).

Focusing our attention on the predominant *Eq* conformer of R3MCP, we note that the **HT** intensities for the first two excited states, essentially vanishing in Figure 2, are much smaller than those of the corresponding **FC** terms. The ratio between the two absolute intensities is **FC/HT** = 269 and 316, for S1 and S2, respectively. The **HT** intensities of the S3, S5 and S6 states are not completely negligible, but still weaker than their **FC** counterparts, with for example **FC/HT** ≈ 100 for S3. The **HT** contribution becomes ten times larger than the corresponding **FC** intensity for the S4 state, and the intense peak at around 165 nm in panel (b) of Figure 2, corresponds indeed to the largest **HT** contribution in whole energy range investigated here.

In the *Ax* conformer (see Table 2), the **HT** intensity for the S1 state is completely negligible, with **FC/HT** greater than 1500, whereas those for S2 and S3 are larger, yet barely visible and still much smaller than the corresponding **FC** intensities, with the ratio increasing to 63 and 20, respectively. As for the *Eq* conformer, the **HT** intensity of the S4 state is larger than the **FC** counterpart. S5 shows an **HT** intensity about half-that of S4, whereas S6 exhibits the largest **HT** effect among the six excited states.

In Table 3, LCM energy shifts and Franck−Condon overlap integrals for the vibrational modes exhibiting a sizable displacement d_a calculated for the *Eq* conformer of R3MCP with the CAM-B3LYP functional are shown. Focus is only on the S1, S2, S5 and S6 states, because they have the largest CD response. The displacements d_a of the equilibrium position along the normal modes on the excited PESs with respect to the ground state, and the energy shift, ΔE, obtained assuming a LCM, are expressed as $d_a = -G_a/\omega_a{}^2$ and $\Delta E = -G_a^2/2\omega_a^2$, respectively, where G_a is the gradient of the excited-state energy. We refer readers to ref 31 for detailed information on the derivation of these relationships.

From Table 3 we can see that, without considering the Duschinsky mixing of the normal modes and the change of the frequencies in the excited states, out of a total of 45 vibrational modes, only less than ten exhibit considerable energy shifts for the four excited states under examination. The 0−0 transition plays a dominant role, with the **FC** integral in most cases very close to 1. A detailed analysis highlights the vibrational modes contributing mostly to the **FC** intensities observed in the spectral region of interest: mode 35, with a frequency of 1806 cm^{-1}, corresponding to the C═O stretch, yields the largest energy shift of all four excited states; modes 8 and 9, with frequencies of 538 and 585 cm^{-1}, respectively, correspond to the C−C bending along the molecular plane; modes 10, 13 and 15, with frequencies of 725, 890 and 951 cm^{-1}, respectively, arise from the C−C bending out of the plane; mode 16, associated to a frequency of 996 cm^{-1}, describes the C−C stretching along the molecular plane; modes 19, and 22 to 27, with frequencies ranging from 1145 to 1347 cm^{-1}, are all associated to bendings of the CH groups coupled with CC stretches within the ring. For the first two excited states, S1 and S2, of both conformers *Eq* and *Ax* a better assignment of the experimental peaks can be obtained by going beyond LCM, and relying on the full harmonic vibronic model, see section 4.2.

4.2. Harmonic AFC Approximation for the S1 and S2 Spectra. The LCM analysis made in the previous sections has permitted already a quite satisfactory assignment of the major features observed in experimental ECD spectra,[12] in particular for the region of wavelengths between 330 and 180 nm, where the contribution of the S1 and S2 states are most easily singled out; see Figure 1. Nevertheless, with the aim of performing a more detailed comparison of the computed spectral profiles with experiment and to provide as precise as possible vibrational assignments of the main observed peaks, we decided to go beyond LCM for the S1 and S2 states, and computed harmonic AFC spectra, including both frequency changes and Duschinsky rotation[21] of the normal modes.[20,23,29] For sake of brevity, in the following these spectra will be simply named "harmonic". As a preliminary step, we performed a geometry optimization and harmonic analysis at the CAM-B3LYP/aug-cc-pVDZ level for both the S1 and S2 states, and for both the *Ax* and *Eq* conformers. Geometry optimization of both conformers in the S1 state reveals a distortion of the ring with a pyramidal arrangement around the carbonilic C atom, as a consequence of the $n \rightarrow \pi^*$ nature of the S0 → S1 transition. Because pyramidalization can take place in two different directions, this finding indicates the existence of a double-well in the potential energy profile. Consequently, constrained optimizations impos-

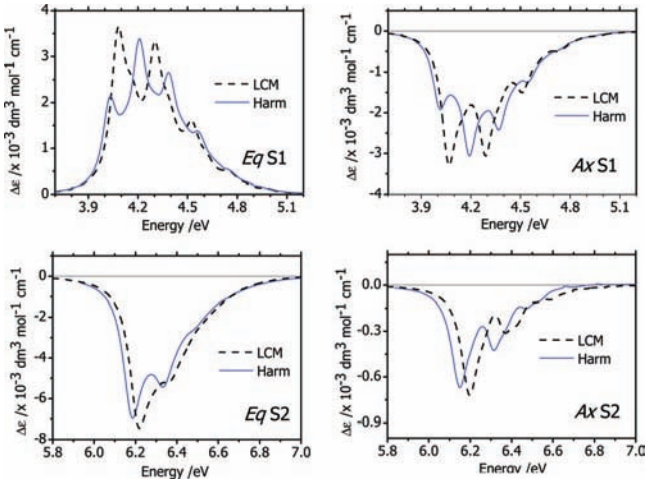

Figure 3. Comparison of the S1 and S2 computed total (**TOT = FC + HT**) ECD spectra of R3MCP, obtained with the linear coupling (LCM) and harmonic AFC (Harm) models, for the two conformers *Ax* and *Eq*. All the spectra have been convoluted with a lorenzian with a lifetime of 0.05 eV.

ing a planar arrangement around the carbonilic C lead to a normal mode with a negative frequency (−240 cm^{-1} for *Ax* and −257 cm^{-1} for *Eq*), corresponding to the pyramidalization motion. Analysis of the Dushinsky matrix **J** further reveals that the S1 mode is mixed to several modes in S0 (to achieve a projection larger than 0.90, six S0 modes are needed for *Ax* and 5 for *Eq*). The largest projection (0.57 for *Ax* and 0.61 for *Eq*) is for sixth S0 mode, whose frequencies are 457 cm^{-1} and 460 cm^{-1}, for *Ax* and *Eq* conformers, respectively. Our focus is here to provide an assignment of the experimental vibrational progression yielding major peaks with a roughly equal spacing of 1215 cm^{-1} (S1). These cannot be due to the double well vibrational states. Therefore we consider an accurate treatment of the pyramidal umbrella motion around the carbonyl (a far from trivial undertaking) beyond the scope of this work. A feasible route to treat this case in the frame of a harmonic HFC approach is described in refs 24 and 25. Within the LCM this mode can simply be neglected, assuming a zero displacement. For harmonic spectra, the situation is more complicated, because the double well modes mix with other normal coordinates (see above) and cannot therefore simply be taken out. In analogy to LCM, for AFC harmonic spectra we assumed a constrained optimal geometry, planar around the carbonilic C, and we set the negative frequency arising from the hindered umbrella motion mode to its absolute value. A different choice, i.e., setting the frequency equal to that of the S0 mode with which it has the largest projection, leads to negligible differences. The effect of neglecting the double-well energy profile on the spectral shape will be further discussed at the end of this section.

Figure 3 reports the comparison of LCM and harmonic spectra (the latter thus including Duschinsky mixing of normal coordinates and the change in frequency of the excited states). Harmonic spectra have been computed by using CAM-B3LYP/aug-cc-pVDZ geometries and normal modes for the excited states, and by refining the excited-state energy minima at CAM-B3LYP/aug-cc-pVTZ level. The LCM and harmonic spectra for S2 are rather similar, apart from a slight blue-shift of the LCM with respect to the harmonic profile. More significant differences appear in the S1 spectra, where the harmonic spectra are significantly red-shifted and their vibrational progression is far more pronounced than predicted at LCM level.

Table 4 reports the frequency and displacement, together with the **FC** factors of class C_1 (a single excited mode in the final

TABLE 4: Frequency (ω_a), Linear Displacement (d_a), and C_1 Class Franck−Condon Factors of the Most Important S1 and S2 Excited-State Vibrational Modes of the Equatorial-Methyl Conformer of R3MCP, Calculated in the Harmonic AFC Approximation by CAM-B3LYP/aug-cc-pVDZ Excited-State Geometry Optimization and Harmonic Analysis[a]

	mode	ω_a (cm^{-1})	d_a (au)	$J_{b_{max}a}{}^2$ [b]	b_{max}	$\lvert\langle \mathbf{0}_g \lvert \mathbf{0}_f + 1_a\rangle\rvert^2$ [c]	$\lvert\langle \mathbf{0}_g \lvert \mathbf{0}_f + 2_a\rangle\rvert^2$ [c]
S1[d]	2	112	15	0.95	1	0.00006	0.00891
	8	514	−7	0.77	8	0.00827	0.00010
	10	787	−11	0.77	10	0.02913	0.00395
	13	913	−3	0.53	13	0.00242	0.00011
	17	1042	−4	0.74	17	0.00483	0.00033
	28	1380	−3	0.80	28	0.00737	0.00015
	30	1449	−17	0.87	35	0.17437	0.09071
	31	1472	−3	0.45	31	0.00455	0.00006
S2[e]	2	160	12	0.99	2	0.01572	0.00007
	4	259	−12	0.96	4	0.02745	0.00022
	7	488	10	0.57	8	0.03841	0.00092
	11	771	−7	0.89	11	0.03043	0.00079
	23	1206	8	0.47	23	0.05153	0.00360
	24	1236	5	0.77	24	0.01961	0.00043
	25	1269	−9	0.68	25	0.05153	0.00360
	28	1375	−4	0.24	28	0.06902	0.00697

[a] For each excited-state mode *a*, the ground-state mode b_{max} on which *a* projects the most ($J_{b_{max}a}{}^2$) is also reported. [b] The square of the matrix element J_{ba} represents the projection of mode *a* of the final state *f* on mode *b* of the initial state *g* (see eq 10). [c] $|\mathbf{0}_g\rangle$ is the ground vibrational state of the ground electronic state *g*, and $|\mathbf{0}_f + \nu_{a,f}\rangle$ is the vibrational state of electronic state *f* with zero quanta on each mode except mode *a* which has ν quanta. [d] The 0−0 **FC** factor for state S1 $|\langle \mathbf{0}_g|\mathbf{0}_1\rangle|^2 = 0.14321$. [e] The 0−0 **FC** factor for state S2 $|\langle \mathbf{0}_g|\mathbf{0}_2\rangle|^2 = 0.31662$.

electronic state)[23] for the more relevant modes in the S1 and S2 ECD spectra of the predominant *Eq* conformer. For each excited-state mode *a* the S0 mode b_{max} on which *a* has the largest projection (the square of the corresponding element of the Duschinky **J** matrix, $J_{b_{max}a}{}^2$) is also reported. In Figure 4 the vibrational assignment of the main stick bands contributing to the S1 and S2 spectra for the predominant *Eq* conformer are reported. Specifically, the quantities $\omega_{g\nu_g f\nu_f} \cdot {}^{g\nu_g f\nu_f}R$ are reported as stick bands at frequency $\omega_{g\nu_g f\nu_f}$. Although the lowest energy peak in the S1 spectrum is mainly assigned to the 0−0 transition between the ground vibrational states of the two electronic states, the other peaks of the harmonic spectrum are associated to a progression along the CO stretch (mode 30), with spacing of 1450 cm^{-1} (for both conformers). Though Table 4 shows that this mode is projected on a single S0 mode (35) for about 87%, the S1 frequency is sensibly smaller than the corresponding S0 one, 1805/1806 cm^{-1} (*Ax*/*Eq*), because the $n \rightarrow \pi^*$ excitation causes a weakening of the CO bond. LCM neglects frequency changes, and therefore it predicts larger spacings between the peaks of the S1 spectra. As expected by inspection of Table 4, a second relevant contribution to the S1 *Eq* spectrum is given by mode 10, describing a concerted out of plane bending of several H atoms bound to the carbon ring.

In the *Eq* spectrum of the S2 state (lower panel of Figure 4), the low energy peak is mainly due to the 0−0 transition, whereas the higher-energy peak intensity results from the contributions of fundamentals of modes 23, 24 and 25. These all correspond to collective CH out-of-plane bendings coupled to stretches of the CC ring bonds. Inspection of Table 4 shows that these modes are also those with larger displacements, for which a longer **FC** progression is expected. A sensible contribution in the energy region between the two peaks of the S2 spectrum is given by the fundamental of mode 7, corresponding to a planarization motion of the ring. The harmonic spectrum of the S2 state of

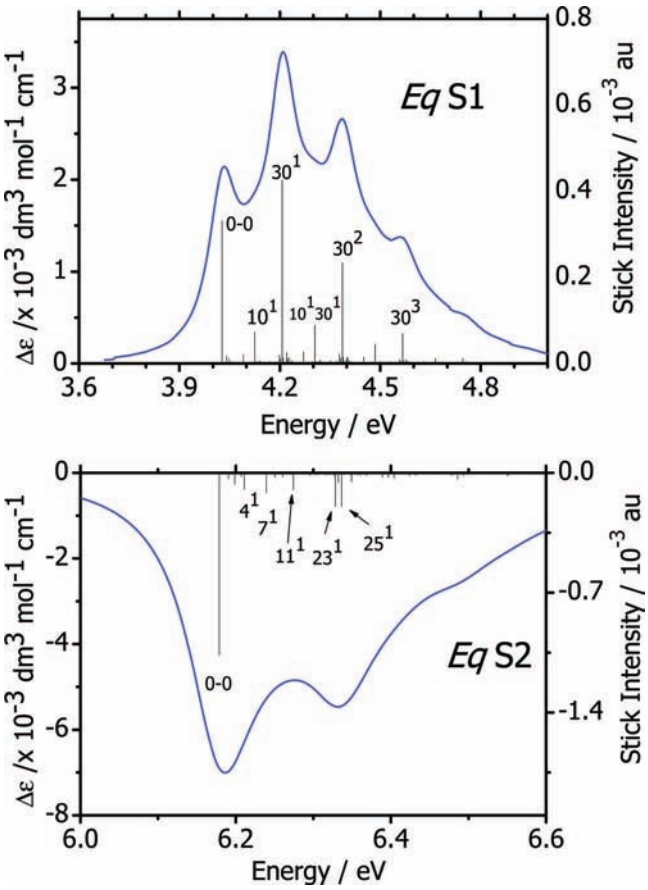

Figure 4. Assignments of the main stick bands of the S1 and S2 harmonic AFC ECD spectra of the predominant *Eq* conformer of R3MCP. Vibrational contributions are labeled ax "n^x", where x indicates the quanta deposited on the excited-state normal mode n. When the x is not explicitly given, it is intended that the corresponding mode is in the ground state ($x = 0$). Combination bands, $n^x m^y$, are indicated in parentheses.

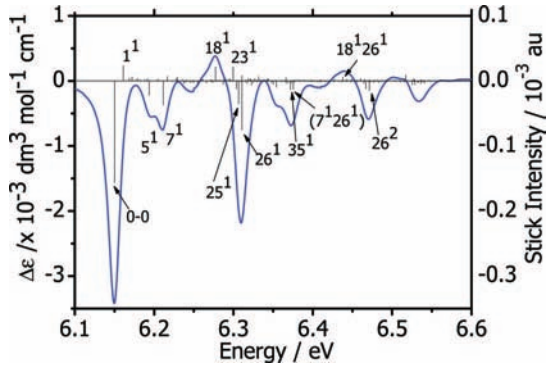

Figure 5. Computed total (**TOT** = **FC** + **HT**) S2 ECD spectrum of the *Ax* conformer of R3MCP, obtained with the harmonic AFC (Harm) model and convoluted with a Lorenzian with a lifetime of 0.01 eV. Also the stick spectrum is reported, and the main bands are assigned ax "n^x", where x indicates the quanta deposited on the excited-state normal mode n. Combination bands are in parentheses.

the *Ax* conformer (see Figure 5) shows a much richer vibrational structure than its *Eq* counterpart, with positive and negative stick bands. This feature is a clear signature of relevant **HT** effects, because at the **FC** level stick bands for a given excited state would all have the same uniform sign. The phenomenon is so relevant as to introduce a change of sign in the high-resolution convoluted spectrum (for a moderate lifetime of 0.01 eV), a feature that disappears for lower-resolution spectra (lifetime of 0.05 eV; see Figure 3). The interesting possibility of a change of sign in ECD spectra of a single electronic state and its consequence for the use of ECD spectra to assign molecular absolute configurations were highlighted and discussed in detail elsewhere.[55] The prediction of ref 55, made on the basis of LCM calculations, is confirmed by the results presented in Figure 5, obtained by the AFC full-harmonic approach.

Figure 6 compares the computed (both LCM and harmonic) and the experimental[12,13] spectra for S1 and S2. Computed spectra have been obtained by averaging over the *Ax* and *Eq* spectra according to the Boltzmann weights given in section 3. For a better comparison of the vibronic profiles, in the lower panels of Figure 6 the S1 (S2) spectra were redrawn after normalization of the highest (lowest) peak to 1 (−1), and the computed spectra were shifted along the energy axis to better superimpose to their experimental counterparts. The amount of the shifts—0.226 eV (S1) and 0.056 eV (S2) for harmonic spectra; 0.279 eV (S1) and 0.024 eV (S2) for LCM spectra—can be used as an estimate of the computational error in the vertical excitation energy. The figures in the upper panel show that the total intensity is reasonably reproduced both by LCM and harmonic calculations, being only slightly underestimated for S1 and overestimated for S2. The lower panel of Figure 6 shows that the comparison of computed and experimental spectra is sensibly improved going from the LCM to a full harmonic model: both the relative height of the peaks and their average spacing are better reproduced. The good agreement between experimental and harmonic profiles allows us to assign the experimental progression to the CO stretch. The spacing of the harmonic spectrum (∼1450 cm^{-1}) is still slightly overestimated with respect to the average spacing of the experimental spectrum (1215 cm^{-1}), thus indicating that the computed S1 CO stretch is essentially overestimated roughly by about 235 cm^{-1}. The residual difference in the relative heights of the computed harmonic and experimental peaks suggests that the predicted elongation of the CO stretch upon the S0−S1 transition—from 1.205 Å to 1.285 Å for *Ax*; from 1.205 Å to 1.303 Å for *Eq*—is also slightly underestimated. A further improvement of the agreement between the experimental and computed spectrum may come from the use of anharmonic frequencies in place of the harmonic ones, according to a recent approach developed by one of us.[56]

As already noted above, the harmonic AFC treatment yields an absolute position of the S1 harmonic spectrum in better agreement with experiment than the LCM (the error is 0.226 eV, compared to 0.289 eV). The opposite holds for the S2 spectrum, where the error of the harmonic spectrum (0.056 eV) is reduced to 0.024 eV at LCM level. As far as the S2 spectral shape is concerned, Figure 6 shows that both LCM and harmonic calculations provide results in good agreement with the experiment, nicely reproducing the ∼1110 cm^{-1} spacing of the two-peak profile (∼1170 cm^{-1} according to the harmonic prediction). The comparison of the relative heights of the two peaks is less satisfactory, because theory appears to underestimate the intensity of the blue peak. The assignments made in Figure 4 indicate that, while the red peak mainly arises from the 0−0 transition, the blue peak is due to the fundamentals of modes 23−25.

The experimental S1 spectrum appears to be broader than the S2 one. This feature is not easily explained on the ground of typical mechanisms both for homogeneous broadening (which should not be larger for S1 than for S2, because highly excited states are expected to have smaller lifetimes) or for inhomogeneous broadening (which should be similar for the

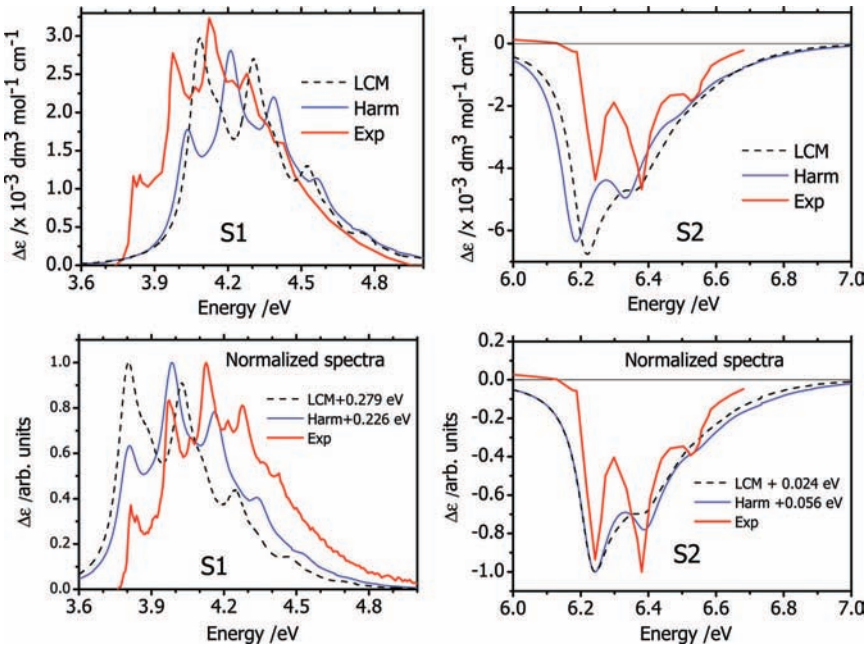

Figure 6. Comparison of the experimental (Exp) ECD spectra of R3MCP in the S1 and S2 regions with the Boltzmann averaged ($T = 298.15$ K, $P = 1$ atm) spectra computed at linear coupling (LCM) and harmonic AFC (Harm) levels. For a better comparison, in the lower panel the spectra were normalized to a maximum (minimum) intensity of 1 (−1) for the S1 (S2) state, respectively, and the computed spectra were shifted on the energy axis by the amount reported in the insets.

TABLE 5: Gibbs Free Energies G_i (+309 au) and Boltzmann Factors X_i Obtained with a B3LYP/aug-cc-pVTZ Method for the Equatorial-Methyl (*Eq*) and Axial-Methyl (*Ax*) Conformers of R3MCP at Different Temperatures (Pressure $P = 1$ atm)

temp (°C)	G_{eq}	G_{ax}	$100X_{ax}$	$100X_{eq}$
20	−0.888947	−0.886884	9.78	90.22
40	−0.891570	−0.889505	11.08	88.92
60	−0.894253	−0.892185	12.35	87.65
80	−0.896997	−0.894926	13.57	86.43

two states, most of all in gas phase).[57] We suggest that the broader S1 spectrum is due to the double-well profile of the PES discussed at the beginning of this section. Indeed, the superposition of the harmonic states along the carbonilic C pyramidalization motion on the ground state, with the anharmonic S1 states due to the double-well PES, are expected to produce a long progression of closely spaced transitions, whose ultimate effect would be the broadening of the spectrum. This phenomenon will be analyzed in detail elsewhere.

4.3. Final Detour: The Temperature Dependence of the Spectral Profiles. In ref 13, Compton and co-workers have extended their previous studies[12] of the optical response of R3MCP to include the temperature-dependence of the ECD spectra, measuring it in different solvents. Experimentally, the determination of the temperature-dependence of the ECD spectrum of R3MCP in the vapor phase is an extremely difficult task, which was not attempted by the authors of refs 12 and 13. In Table 5, Gibbs free energies, computed B3LYP/aug-cc-pVTZ, as well as Boltzmann factors for the gaseous *Eq* and *Ax* conformers at four different temperatures ranging from 20 to 80 °C ($P = 1$ atm) are reported. The temperatures are those chosen by Li and co-workers for their experimental study presented in ref 12. There the *T*-dependence of the ECD spectra was investigated in cyclohexane, whose static dielectric constant is $\epsilon = 2.02$ and whose solvent effect on the optical response of its solute was often found to be negligible,

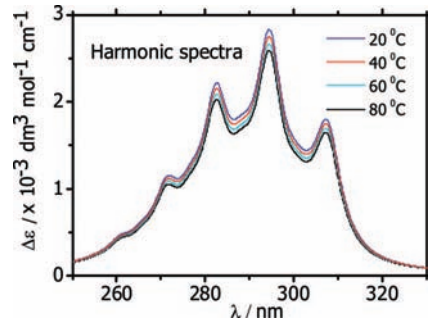

Figure 7. Boltzmann averaged vibronically resolved circular dichroism spectra of R3MCP at different temperatures for the first excited state, the $n \rightarrow \pi^*$ band wavelength region, calculated with CAM-B3LYP/aug-cc-pVTZ employing B3LYP/aug-cc-pVTZ optimized geometries. The harmonic AFC vibronic model has been employed. Only the total spectra (resulting from the combination of Franck−Condon and Herzberg−Teller contributions) are shown with lifetime broadening of 0.05 eV.

yielding properties very close to those expected and measured in the pure vapor phase. In Figure 7 the Boltzmann averaged harmonic vibronic CD profiles calculated with the CAM-B3LYP functional as a function of the temperature are shown. The total spectra, combining **FC** and **HT** contributions, with lifetime of 0.05 eV are shown. Attention is focused on the S1 region, as in experiment,[12,13] where the $n \rightarrow \pi^*$ transition occurs. The intensity of the CD decreases as the temperature of the sample increases, reproducing the experimental observations. Table 5 shows that the population of the *Ax* conformer increases at the expense of the *Eq* conformer as the temperature increases. This, together with the fact that the *Eq* conformer yields a positive response in the region of interest, whereas the *Ax* signal is negative, easily explains the evidence.

5. Conclusions

We presented the results of density functional response theory simulations for the vibronic profiles of CD for a typical

chiral molecule, (*R*)-(+)-3-methylcyclopentanone, in the vapor phase. The Boltzmann averaged spectrum calculated with the recently developed CAM-B3LYP functional well reproduces the experimental spectra, with an excellent performance for both the position and the intensity of the dichroic peaks. Both the Franck−Condon and Herzberg−Teller contributions to the electronic CD response of the first six excited states have been analyzed by resorting to a linear coupling model, and the response of the first two S1 and S2 excited states has been also analyzed in deeper detail by AFC harmonic calculations, including frequency changes and Duschinsky mixing of the normal coordinates. The remarkable agreement between computed and experimental spectra has allowed us to confidently assign the main vibrational structure of the experimental bands by means of our computed harmonic spectra. Though the peaks in the spectral profile arising from S1 are due to a progression along the CO stretch, the two-peak shape of the S2 spectrum is mainly due to the **FC/HT** contributions of the fundamentals of collective CH bendings coupled to stretches of the CC bonds within the ring. The temperature-dependence of the vibronic CD band due to $n \rightarrow \pi^*$ low lying transition has been studied in a range of temperatures corresponding to that employed in experimental studies performed in cyclohexane solutions.[12,13] The intensity decrease of the narrow band observed by Li and co-workers[12] is well reproduced.

Acknowledgment. This work is supported by Swedish Research Council (V.R.) and National Nature Science Foundation of China (20473046). A grant of computer time from the Norwegian Supercomputing Program and computer resources provided by the network Village (http://village.unina.it) are also acknowledged.

References and Notes

(1) Nakanishi, K.; Berova, N.; Woody, R. W. *Circular dichroism: principles and applications*; VCH Publishers Inc.: New York, 1994.

(2) Barron, L. D. *Molecular Light Scattering and Optical Activity*; Cambridge University Press: Cambridge, 2004.

(3) Caldwell, D. J.; Eyring, H. *The Theory of Optical Activity*; Wiley-Interscience: New York, 1971.

(4) Holland, K. D.; Naritoku, D. K.; McKeon, A. C.; Ferrendelli, J. A.; Covey, D. F. *Mol. Pharmacol.* **1990**, *37*, 98.

(5) Polavarapu, P. L.; Bose, P. K.; Hecht, L.; Barron, L. D. *J. Phys. Chem.* **1993**, *97*, 11211.

(6) Polavarapu, P. L.; Zhao, C. *Chem. Phys. Lett.* **1998**, *296*, 105.

(7) Polavarapu, P. L. *Chirality* **2002**, *14*, 768. Erratum *Chirality* **2003**, *15*, 284.

(8) He, J.; Petrovic, A. G.; Polavarapu, P. L. *J. Phys. Chem. B* **2004**, *108*, 20451.

(9) Wellman, K. M.; Bunnenberg, E.; Djerassi, C. *J. Am. Chem. Soc.* **1963**, *85*, 1870.

(10) Richardson, F. S.; Shillady, D. D.; Bloor, J. E. *J. Phys. Chem.* **1971**, *75*, 2466.

(11) Johnson, W. C., Jr. *Rev. Sci. Instrum.* **1971**, *42*, 1283.

(12) Li, R.; Sullivan, R.; Al-Basheer, W.; Pagni, R. M.; Compton, R. N. *J. Chem. Phys.* **2006**, *125*, 144304.

(13) Al-Basheer, W.; Pagni, R. M.; Compton, R. N. *J. Phys. Chem. A* **2007**, *111*, 2293.

(14) Rizzo, A.; Lin, N.; Ruud, K. *J. Chem. Phys.* **2008**, *128*, 164312.

(15) Neugebauer, J.; Baerends, E. J.; Noojien, M.; Autschbach, J. *J. Chem. Phys.* **2005**, *122*, 234305.

(16) Nooijen, M. *Int. J. Quantum Chem.* **2006**, *106*, 2489.

(17) Dierksen, M.; Grimme, S. *J. Chem. Phys.* **2006**, *124*, 174301.

(18) Condon, E. U. *Rev. Mod. Phys.* **1937**, *55*, 2789.

(19) Craig, D. P.; Thirunamachandran, T. *Molecular Quantum Electrodynamics. An Introduction to Radiation Molecule Interaction*; Dover Publications, Inc.: Mineaol, NY, 1984.

(20) Santoro, F.; Improta, R.; Lami, A.; Bloino, J.; Barone, V. *J. Chem. Phys.* **2008**, *128*, 224311.

(21) Duschinsky, F. *Acta Physicochim.* **1937**, *7*, 551.

(22) Peluso, A.; Santoro, F.; Del Re, G. *Int. J. Quantum Chem.* **1997**, *63*, 233.

(23) Santoro, F.; Improta, R.; Lami, A.; Bloino, J.; Barone, V. *J. Chem. Phys.* **2007**, *126*, 084509. *J. Chem. Phys.* **2007**, *126*, 169903.

(24) Hazra, A.; Chang, H. H.; Nooijen, M. *J. Chem. Phys.* **2004**, *121*, 2125.

(25) Hazra, A.; Nooijen, M. *Phys. Chem. Chem. Phys.* **2005**, *7*, 1759.

(26) Kupka, H.; Cribb, P. H. *J. Chem. Phys.* **1986**, *85*, 1303.

(27) Sharp, T. E.; Rosenstock, H. M. *J. Chem. Phys.* **1964**, *41*, 3453.

(28) Doktorov, E. V.; Malkin, I. A.; Man'ko, V. I. *J. Mol. Spectrosc.* **1977**, *64*, 302.

(29) Santoro, F.; Lami, A.; Improta, R.; Barone, V. *J. Chem. Phys.* **2007**, *126*, 184102.

(30) Santoro, F. **FC***classes*, a Fortran 77 code; see http://village.ipcf.cnr.it.

(31) Macak, P.; Luo, Y.; Norman, P.; Ågren, H. *Chem. Phys. Lett.* **2000**, *330*, 447.

(32) Lin, N.; Zhao, X.; Rizzo, A.; Luo, Y. *J. Chem. Phys.* **2007**, *126*, 244509.

(33) Macak, P.; Luo, Y.; Norman, P.; Ågren, H. *J. Chem. Phys.* **2000**, *113*, 7055.

(34) Wang, Y.-H.; Halik, M.; Wang, C.-K.; Marder, S. R.; Luo, Y. *J. Chem. Phys.* **2005**, *123*, 194311.

(35) Minaev, B.; Wang, Y.-H.; Wang, C.-K.; Luo, Y.; Ågren, H. *Spectrochim. Acta Part A* **2006**, *65*, 308.

(36) Cesar, A.; Ågren, H.; Brito, A.; Baltzer, P.; Keane, M.; Svensson, S.; Karlsson, L.; Fournier, P.; Fournier, M. *J. Chem. Phys.* **1990**, *93*, 918.

(37) Gierschner, J.; Mack, H.-G.; Egelhaaf, H.-J.; Schweizer, S.; Doser, B.; Oelkrug, D. *Synth. Met.* **2003**, *138*, 311.

(38) Gierschner, J.; Mack, H.-G.; Lüer, L.; Oelkrug, D. *J. Chem. Phys.* **2002**, *116*, 8596.

(39) Frisch, M. J.; Trucks, G. W.; Schlegel, H. B.; Scuseria, G. E.; Robb, M. A.; Cheeseman, J. R.; Montgomery, J. A., Jr.; Vreven, T.; Kudin, K. N.; Burant, J. C.; Millam, J. M.; Iyengar, S. S.; Tomasi, J.; Barone, V.; Mennucci, B.; Cossi, M.; Scalmani, G.; Rega, N.; Petersson, G. A.; Nakatsuji, H.; Hada, M.; Ehara, M.; Toyota, K.; Fukuda, R.; Hasegawa, J.; Ishida, M.; Nakajima, T.; Honda, Y.; Kitao, O.; Nakai, H.; Klene, M.; Li, X.; Knox, J. E.; Hratchian, H. P.; Cross, J. B.; Bakken, V.; Adamo, C.; Jaramillo, J.; Gomperts, R.; Stratmann, R. E.; Yazyev, O.; Austin, A. J.; Cammi, R.; Pomelli, C.; Ochterski, J. W.; Ayala, P. Y.; Morokuma, K.; Voth, G. A.; Salvador, P.; Dannenberg, J. J.; Zakrzewski, V. G.; Dapprich, S.; Daniels, A. D.; Strain, M. C.; Farkas, O.; Malick, D. K.; Rabuck, A. D.; Raghavachari, K.; Foresman, J. B.; Ortiz, J. V.; Cui, Q.; Baboul, A. G.; Clifford, S.; Cioslowski, J.; Stefanov, B. B.; Liu, G.; Liashenko, A.; Piskorz, P.; Komaromi, I.; Martin, R. L.; Fox, D. J.; Keith, T.; Al-Laham, M. A.; Peng, C. Y.; Nanayakkara, A.; Challacombe, M.; Gill, P. M. W.; Johnson, B.; Chen, W.; Wong, M. W.; Gonzalez, C.; Pople, J. A. *Gaussian 03*, revision D.01; Gaussian, Inc.: Wallingford, CT, 2004.

(40) Becke, A. D. *J. Chem. Phys.* **1993**, *98*, 5648.

(41) Becke, A. D. *Phys. Rev. A* **1988**, *38*, 3098.

(42) Lee, C.; Yang, W.; Parr, R. G. *Phys. Rev. B* **1988**, *37*, 785.

(43) Yanai, Y.; Tew, D. P.; Handy, N. C. *Chem. Phys. Lett.* **2004**, *393*, 51.

(44) Peach, M. J. G.; Helgaker, T.; Salek, P.; Keal, T. W.; Lutnaes, O. B.; Tozer, D. J.; Handy, N. C. *Phys. Chem. Chem. Phys.* **2006**, *8*, 558.

(45) DALTON, a molecular electronic structure program, Release 2.0 (2005), see http://www.kjemi.uio.no/software/dalton/dalton.html.

(46) Frisch, M. J.; Trucks, G. W.; Schlegel, H. B.; Scuseria, G. E.; Robb, M. A.; Cheeseman, J. R.; Montgomery, J. A., Jr.; Vreven, T.; Scalmani, G.; Mennucci, B.; Barone, V.; Petersson, G. A.; Caricato, M., Nakatsuji, H.; Hada, M.; Ehara, M.; Toyota, K.; Fukuda, R.; Hasegawa, J.; Ishida, M.; Nakajima, T.; Honda, Y. Kitao. O.; Nakai, H.; Li, X.; Hratchian, H. P.; Peralta, J. E.; Izmaylov, A. F.; Kudin, K. N.; Heyd, J. J.; Brothers, E.; Staroverov, V.; Zheng, G.; Kobayashi, R.; Normand, J.; Sonnenberg, J. L.; Iyengar, S. S.; Tomasi, J.; Cossi, M.; Rega, N.; Burant, J. C.; Millam, J. M.; Klene, M.; Knox, J. E.; Cross, J. B.; Bakken, V.; Adamo, C.; Jaramillo, J.; Gomperts, R.; Stratmann, R. E.; Yazyev, O.; Austin, A. J.; Cammi, R.; Pomelli, C.; Ochterski, J. W.; Ayala, P. Y.; Morokuma, K.; Voth, G. A.; Salvador, P.; Dannenberg, J. J.; Zakrzewski, V. G.; Dapprich, S.; Daniels, A. D.; Strain, M. C.; Farkas, O.; Malick, D. K.; Rabuck, A. D.; Raghavachari, K; Foresman, J. B.; Ortiz, J. V.; Cui, Q.; Baboul, A. G.; Clifford, S.; Cioslowski, J.; Stefanov, B. B.; Liu, G.; Liashenko, A.; Piskorz, P.; Komaromi, I.; Martin, R. L.; Fox, D. J.; Keith, T.; Al-Laham, M. A.; Peng, C. Y.; Nanayakkara, A.; Challacombe, M.; Chen, W.; Wong, M. W.; Pople, J. A. *Gaussian*; Gaussian, Inc.: Wallingford, CT, 2006.

(47) Note that there is a misprint in ref 14. The column of ECD rotational strengths for CAM-B3LYP/aug-cc-pVTZ is erroneously identical to that given for B3LYP/aug-cc-pVTZ. The CAM-B3LYP/aug-cc-pVTZ should be substituted by the following: 14.534;−14.741; 0.956; 0.355; 4.892; 14.871. The residual differences with respect to those in Table 1 in the present work are due to the fact that the original geometry, taken from ref 8, has been re-optimized for this study.

(48) O'Toole, L.; Brint, P.; Kosmidis, C.; Boulakis, G.; Bolovinos, A. *J. Chem. Soc., Faraday Trans.* **1992**, *88*, 1237.

(49) Skomorowski, W.; Pecul, M.; Sałek, P.; Helgaker, T. *J. Chem. Phys.* **2007**, *127*, 085102.
(50) Solheim, H.; Frediani, L.; Ruud, K.; Coriani, S. *Theor. Chim. Acta* **2008**, *119*, 231.
(51) Shcherbin, D.; Ruud, K. *Chem. Phys.* **2008**, *349*, 234.
(52) Herzberg, G.; Teller, E. *Z. Phys. Chem.* **1933**, *B21*, 410.
(53) Fulton, R. L. *J. Chem. Phys.* **1972**, *56*, 1210.
(54) Orlandi, G.; Siebrand, W. *J. Chem. Phys.* **1973**, *58*, 4513.
(55) Lin, N.; Luo, Y.; Santoro, F.; Zhao, X.; Rizzo, A. *Chem. Phys. Lett.* **2008**, *464*, 144.
(56) Bloino, J.; Biczysko, M.; Crescenzi, O.; Barone, V. *J. Chem. Phys.* **2008**, *128*, 244105.
(57) Levine, E. N. *Molecular Spectroscopy*; Wiley Interscience: New York, 1975.

JP8064695